GRAIL Gravity Field Determination Using the Celestial Mechanics Approach - Status Report

EGU2015-13226
European Geosciences Union
General Assembly 2015
12 - 17 April 2015, Vienna, Austria

D. Arnold, S. Bertone, A. Jäggi, G. Beutler, L. Mervart

Astronomical Institute, University of Bern, Bern, Switzerland

Introduction

To determine the gravity field of the Moon, the two satellites of the NASA mission GRAIL (Gravity Recovery and Interior Laboratory) were launched on September 10, 2011 and reached their lunar orbits in the beginning of 2012 (Zuber et al., 2013). The concept of the mission was inherited from the Earth-orbiting mission GRACE (Gravity Recovery and Climate Experiment) in that the key observations consisted of ultra-precise inter-satellite Ka-band range measurements. Together with the one- and two-way Doppler observations from the NASA Deep Space Network (DSN), the GRAIL data allows for a determination of the lunar gravity field with an unprecedented accuracy for both the near- and the far-side of the Moon. The latest official GRAIL gravity field models contain spherical harmonic (SH) coefficients up to degree and order 900 (Konopliv et al., 2014, Lemoine et al., 2014).

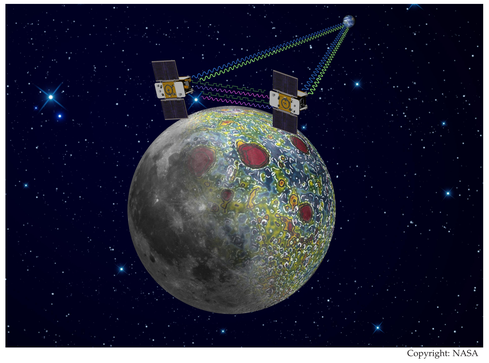

Copyright: NASA

Based on our experience in GRACE data processing, we are adapting our approach for gravity field recovery, the Celestial Mechanics Approach (CMA, Beutler et al., 2010), to the GRAIL mission within the Bernese GNSS software. We use the level 1b Ka-band range-rate (KBRR) data as original observations and - since the implementation of DSN data analysis into the Bernese GNSS software is still under development - the dynamic GNI1B position data as pseudo-observations (relative weighting $10^8 : 1$). The following results are based on the release 4 data of the primary mission phase (PM, 1 March to 29 May 2012).

The Celestial Mechanics Approach (CMA)

The idea of the CMA is to rigorously treat the gravity field recovery as an extended orbit determination problem. It is a dynamic approach allowing for appropriately constrained stochastic pulses (instantaneous changes in velocity) to compensate for inevitable model deficiencies. For each satellite, the equations of motion to be solved read as $\ddot{\mathbf{r}} = \mathbf{a}_G + \mathbf{a}_P$, where $\mathbf{a}_G = \nabla V$ denotes the acceleration due to the gravity potential V, which we parametrize in terms of the standard SH expansion. $\mathbf{a}_P$ denotes the sum of all perturbing accelerations. We consider 3rd body perturbations according to JPL ephemerides DE421, forces due to the tidal deformation of the Moon and relativistic corrections. We do not yet model direct or indirect solar radiation pressure explicitly.
All observations contribute to one and the same set of parameters, which are simultaneously estimated. In our case, these are:

- Orbits: Initial conditions every 24h; once-per-revolution accelerations in R,S,W (radial, along-track, out-of-plane); stochastic pulses in R,S,W every $40'$.
- Static gravity field: The coefficients of the SH expansion up to degree and order 200.
- Ka-band: Time bias every 24h.

Orbits

In a first step, we estimate a priori orbits using the GNI1B positions and KBRR observations. Fig. 1 shows that their quality strongly depends on the a priori gravity field used.

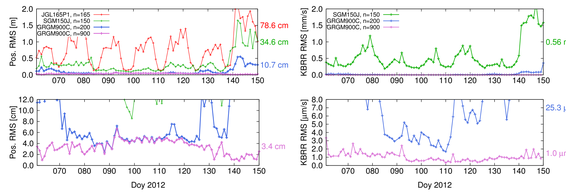

Figure 1: Left: RMS values of the GNI1B position fit. Right: RMS values of the KBRR residuals in the combined (position and Ka-band) orbit solution. Lower plots are zooms of upper ones. The fits are relatively bad when using the Lunar Prospector (JGL165P1) or SELENE (SGM150J) gravity field and become better (more consistent) when introducing NASA's official GRAIL field GRGM900C (Lemoine et al., 2014), truncated at the degrees indicated.

Fig. 2 (left) shows Ka-band residuals for day 062. The gravity field GRGM900C was used up to degree and order 660. Compared to the expected noise level of around 0.05 μm/s, the residuals are still relatively large and clearly show the occurrence of pseudo-stochastic pulses. The green and blue bars indicate the time spans during which each satellite is in sunlight. The obvious correlation between these time spans and the large discontinuities suggests that radiation pressure modeling is crucial. In the analysis of release 2 data, it was necessary to estimate a Ka-band time bias (*i.e.*, an offset of the Ka-band observation epoch from the nominal one); its impact turned out to be negligible for release 4 (see Fig. 2 right).

Figure 2: Left: KBRR residuals and time spans for which GRAIL-A (green) and GRAIL-B (blue) are in sunlight. Vertical black lines indicate locations of pseudo-stochastic pulses. Right: The estimated Ka-band time biases for release 2 (red) and release 4 (green), the latter **shifted by -1.02 s** to have them in the same plot.

Gravity field

We set up stochastic pulses every 40 minutes. This value is a compromise between making up for model deficiencies and not absorbing too much of the gravity signal. The orbits determined in the first step serve as a priori orbits for a common orbit and gravity field estimation based on daily arcs.

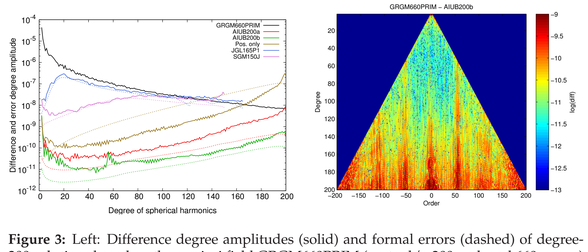

Figure 3: Left: Difference degree amplitudes (solid) and formal errors (dashed) of degree-200 solutions based on the a priori field GRGM660PRIM (up to d/o 200, red, and 660, green) compared to pre-GRAIL solutions. The orange curve represents a position-only solution. Right: Coefficient differences between GRGM660PRIM and AIUB200b.

A classical least-squares adjustment is used. The daily normal equation systems (NEQs) are stacked to weekly, monthly and finally three-monthly NEQs, which are then inverted.

Fig. 3 (left) shows the difference degree amplitudes of our degree-200 solutions AIUB200a and AIUB200b, which use GRGM660PRIM (NASA's previous official GRAIL field) as a priori field up to d/o 200 and 660, respectively. The latter illustrates the impact of the omission error on our solutions. The consistency between AIUB200b and GRGM660PRIM markedly drops around degree 55. The triangle plot of the coefficient differences in Fig. 3 (right) reveals that the coefficients of order ∼55 (as well as the zonal terms) are degraded. The reason for this issue is not yet clear.

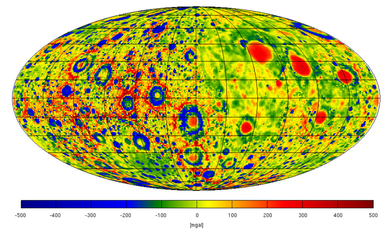

Figure 4: Free-air gravity anomalies of AIUB200b on a $0.5° \times 0.5°$ grid. Mollweide projection centered around 270°, with the nearside on the right.

In addition, a position-only solution was computed. The orange curve in Fig. 3 (left) shows that the gravity field solutions are dominated by the GNI1B positions only at the very lowest degrees and that the KBRR data strongly improves them.
Fig. 5 (left) shows difference degree amplitudes of solutions obtained with the indicated a priori fields. When starting with JGL165P1, after the 2nd iteration the solution matches almost perfectly the solution obtained when using GRGM900C up to d/o 120 as a priori field. This proves the relative insensitivity of the CMA for the used a priori field and justifies the use of GRGM660PRIM as a priori field for AIUB200a/b.
As further validation of our results, we computed the correlation between gravity and topography (Wieczorek , 2007). We used the lunar topography derived from the Lunar Orbiter Laser Altimeter (LOLA) to compute the topography-induced gravity. Fig. 5 (right) shows that correlation for our solution AIUB200a is comparable to the correlation for GRGM660PRIM up to degree 160. The decrease for higher degrees is then mainly due to the omission error.

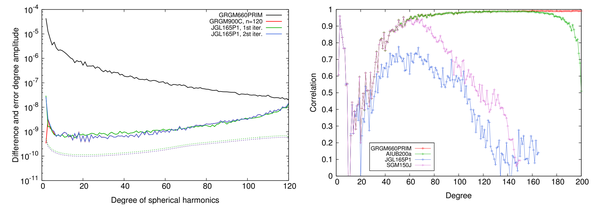

Figure 5: Left: Difference degree amplitudes of solutions obtained from the a priori fields indicated. Right: Correlation between the gravity field induced by the LOLA lunar topography and different lunar gravity fields.

Doppler data processing

Besides the KBRR observations, GRAIL orbit and gravity field determination is based on its Doppler tracking by several Earth-based stations of the DSN. The observed signal is the frequency registered at the tracking station based on the travel time of a series of radio signals between the satellite and the DSN station over a given "counting interval".
In order to process GRAIL Doppler observations, we then need an analytical model of light propagation including

- the trajectory of the tracking station and an a priori orbit for the GRAIL satellites (e.g., based on GNI1B positions) in a common reference frame (we use the Barycentric Celestial Reference Frame),
- a modeling of biases and non-geometrical effects in the Doppler signal (atmospheric delay, etc.) as well as GRAIL attitude information and precise planetary ephemeris.

Moreover, we model relativistic time-scales transformations and we introduce a frequency bias for one-way data. Fig. 6 shows the current status of our pre-fit Doppler residuals based on GNI1B-derived orbits of GRAIL-A and GRAIL-B and the Doppler data. Observations are screened for outliers by setting a threshold on the residuals and by applying an elevation cutoff at 25°.

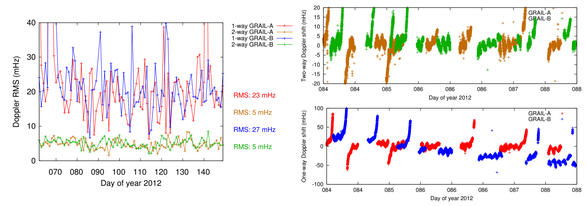

Figure 6: Left: Daily RMS of one-way and two-way Doppler residuals for both GRAIL-A and GRAIL-B over the PM. Right: Detail of one-way and two-way Doppler residuals over days 084-088. The "spikes" at the boundaries of some orbital passes are still under investigation.

Based on screened Doppler data, we recently generated our first orbit solution for GRAIL. We used the GRGM900C field up to d/o 200 and a classical least-square fit to improve six initial orbital elements from the so called "navigation orbit" solution in daily arcs. Fig. 7 shows the difference (as daily RMS of the local orbital frame components) of our solution w.r.t. a fit of the GNI1B positions performed with the same models.

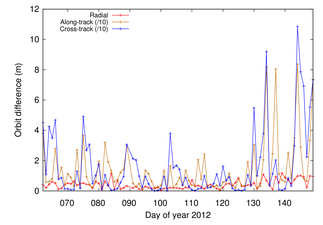

Figure 7: Comparison (as daily RMS of the difference) of GRAIL-A orbits generated over the PM by a fit of Doppler and GNI1B positions, respectively.

Conclusions

- The adaption of the CMA from GRACE to GRAIL allows for good quality lunar gravity fields obtained with the Bernese GNSS software.
- Our gravity field solutions are so far computed without modeling non-gravitational forces at all and demonstrate the potential of pseudo-stochastic orbit parametrization. To fully exploit the precision of the Ka-band observations, we will now set the focus on empirical and analytical solar radiation pressure modeling.
- While further improving our Doppler modeling, we processed preliminary orbit solutions based on Doppler data within the Bernese GNSS software. Further analysis, the improvement of the force modeling and the introduction of additional empirical parameters are needed before using these orbits for gravity field determination.

References

Beutler et al. (2010) *The celestial mechanics approach: theoretical foundations*. J Geod 84:605-624 and *The celestial mechanics approach: application to data of the GRACE mission*. J Geod 84:661-681
Konopliv et al. (2014) *High-resolution lunar gravity fields from the GRAIL Primary and Extended Missions*. Geophys. Res. Letters 41, 1452-1458
Lemoine et al. (2014) *GRGM900C: A degree 900 lunar gravity model from GRAIL primary and extended mission data*. Geophys. Res. Letters 41, 3382-3389
Moyer (2000) *Formulation for Observed and Computed Values of Deep Space Network Data Types for Navigation*. JPL Publications
Wieczorek (2007) *Gravity and topography of the terrestrial planets*. Treatise on Geophysics 10, 165-206
Zuber et al. (2013) *Gravity field of the moon from the gravity recovery and interior laboratory (GRAIL) mission*. Science, 339(6120), 668-671

Contact address

Daniel Arnold
Astronomical Institute, University of Bern
Sidlerstrasse 5
3012 Bern (Switzerland)
daniel.arnold@aiub.unibe.ch

Poster compiled by Daniel Arnold, April 2015
Astronomical Institute, University of Bern, Bern
daniel.arnold@aiub.unibe.ch